

Density matrix approach to the complex heavy ion optical potential

R. Sartor and Fl. Stancu

Institut de Physique B5, Université de Liège, Sart Tilman, B-4000 Liège 1, Belgium

(Received 28 April 1982)

We extend the applicability of the density matrix expansion to a complex effective interaction depending both on the density and the kinetic energy density. A detailed study of the kinetic energy density dependence of the density matrix expansion coefficients is given. The corresponding energy density has a parametrized form which is tested in the calculation of the optical potential of the $^{16}\text{O} + ^{16}\text{O}$ system at several energies. Exact results are well reproduced by the complex density matrix expansion.

[NUCLEAR REACTIONS Density matrix expansion for a complex effective interaction; application to heavy ion optical potential.]

I. INTRODUCTION

It is now common practice¹⁻¹⁴ to define the heavy ion optical potential at a separation distance D as the difference between the expectation value of some effective Hamiltonian H at distance D and the expectation value of the same Hamiltonian at infinity

$$V_{\text{opt}}(D) = \langle H(D) \rangle - \langle H(\infty) \rangle. \quad (1.1)$$

Early computations¹⁻⁶ used an energy functional or an effective interaction which can be related to G matrix calculations in nuclear matter with a spherical Fermi sea. As a consequence those computations could only determine the real part of the optical potential. However, if the heavy ion collision is locally described as the collision of two nuclear matter systems,⁷⁻²⁰ one is led to a non-Hermitian G matrix^{7,8,10-14,20} which will also enable the computation of $\text{Im}V_{\text{opt}}(D)$ through the use of Eq. (1.1).

The direct computation of V_{opt} from a finite range effective interaction is, however, cumbersome and time consuming. As a consequence, approximation schemes have been proposed. A convenient procedure, extensively used for the real part¹⁻⁶ of V_{opt} , is based on energy functionals. In a previous work²¹ we proposed a complex Skyrme-type interaction which generates a complex energy density, to be used in the calculation of both the real and imaginary parts. The imaginary part of the Skyrme-type interaction was obtained by multiplying the real Skyrme-interaction used in Ref. 3 by a scaling factor. This was assumed to depend on the local density ρ and the intrinsic kinetic energy density $\tau^{(2)}$ and found numerically from the finite range complex ef-

fective interaction of Ref. 12.

In Ref. 14, more emphasis was put on avoiding the explicit use of any wave function in the computation of the expectation values appearing in Eq. (1.1). Suitable approximations for ρ and $\tau^{(2)}$ have been found to reproduce the exact results at low energies by means of a generalized double folding method.

In this paper we extend the density matrix expansion (DME) of Negele and Vautherin²² to the complex domain in order to justify the energy functional introduced in Ref. 21.

The present paper is organized as follows. In Sec. II, we briefly recall the DME and single out the peculiar features arising from its application to a complex effective interaction. In Sec. III, we discuss the asymptotic behavior of two colliding nuclear matter systems when the Fermi sea is nearly spherical, and its consequences on the imaginary part of the optical potential. In Sec. IV, we provide a parametrized form for the DME coefficients, and in Sec. V we apply it to the calculation of the optical potential of the $^{16}\text{O} + ^{16}\text{O}$ system and compare the present results with the exact calculations of Ref. 13.

II. THE DENSITY MATRIX EXPANSION WITH A COMPLEX EFFECTIVE INTERACTION

In this section, we recall the relevant DME formulas derived in Ref. 22 and adapt them to the case of a complex effective interaction. The discussion is limited to nuclei having an equal number of neutrons and protons. The effective N - N interaction

which we use in this paper is the spin S and isospin T dependent force derived in Ref. 12. Each ST component can be written as

$$v^{ST}(r) = \frac{1}{x} (1 - e^{-2x})^2 e^{-3x} \sum_{m=0}^6 A_m^{ST} x^m \quad \text{for } r < 1 \text{ fm}, \quad (2.1)$$

$$= \frac{1}{x} (1 - e^{-2x})^2 \sum_{m=1}^7 Z_m^{ST} e^{-mx} \quad \text{for } r > 1 \text{ fm}, \quad (2.2)$$

with $x = 0.7r$, where r is the separation distance between the interaction nucleons, and A_m^{ST} and Z_m^{ST} are complex coefficients depending upon the local density ρ , the local intrinsic kinetic energy density $\tau^{(2)}$ defined in Sec. III, and the incident energy (see Refs. 10–14 for full details).

The basic approximation of the DME proposed in Ref. 22 was to use the following truncated Bessel function expansion for the density matrix:

$$\rho \left[\vec{\mathbf{R}} + \frac{\vec{\mathbf{s}}}{2}, \vec{\mathbf{R}} - \frac{\vec{\mathbf{s}}}{2} \right] = \rho_{SL}(k_{FS}) \rho(\vec{\mathbf{R}}) + \frac{35}{2sk_F^3} \times j_3(k_{FS}) \left[\frac{1}{4} \nabla^2 \rho(\vec{\mathbf{R}}) - \tau(\vec{\mathbf{R}}) + \frac{3}{5} k_F^2 \rho(\vec{\mathbf{R}}) \right], \quad (2.3)$$

$$V_{NM} = \frac{\rho^2}{32} \int d^3s [3v^{TE}(s) + 3v^{SE}(s) + 9v^{TO}(s) + v^{SO}(s)] + \frac{\rho^2}{32} \int d^3s \rho_{SL}^2(k_{FS}) [3v^{TE}(s) + 3v^{SE}(s) - 9v^{TO}(s) - v^{SO}(s)] \quad (2.8)$$

is the potential energy of nuclear matter corresponding to the local density $\rho(\vec{\mathbf{R}})$, and V_D and V_E are the direct (D) and exchange (E) finiteness corrections given by

$$V_D = \frac{1}{32} \int d^3s s^2 g(k_{FS}) [3v^{TE}(s) + 3v^{SE}(s) + 9v^{TO}(s) + v^{SO}(s)] \quad (2.9)$$

and

$$V_E = \frac{1}{16} \int d^3s s^2 \rho_{SL}(k_{FS}) g(k_{FS}) \times [3v^{TE}(s) + 3v^{SE}(s) - 9v^{TO}(s) - v^{SO}(s)] \quad (2.10)$$

where $\rho(\vec{\mathbf{R}})$ and $\tau(\vec{\mathbf{R}})$ are, respectively, the matter and kinetic energy densities at point $\vec{\mathbf{R}}$, and $\rho_{SL}(k_{FS})$ is the Slater approximation given by

$$\rho_{SL}(k_{FS}) = \frac{3}{sk_F} j_1(k_{FS}). \quad (2.4)$$

In Eqs. (2.3) and (2.4), the local Fermi momentum k_F is related to the matter density $\rho(\vec{\mathbf{R}})$ by

$$k_F = \left[\frac{3\pi^2}{2} \rho(\vec{\mathbf{R}}) \right]^{1/3}. \quad (2.5)$$

By writing a similar expansion for the product

$$\rho \left[\vec{\mathbf{R}} + \frac{\vec{\mathbf{s}}}{2} \right] \rho \left[\vec{\mathbf{R}} - \frac{\vec{\mathbf{s}}}{2} \right],$$

which appears in the direct term of the expectation value $\langle H \rangle$, one can express the potential part of $\langle H \rangle$ as²²:

$$\langle H \rangle_{\text{pot}} = \int \mathcal{H}_{\text{pot}}(\vec{\mathbf{R}}) d\vec{\mathbf{R}}, \quad (2.6)$$

where the potential energy density $\mathcal{H}_{\text{pot}}(\vec{\mathbf{R}})$ reads:

$$\mathcal{H}_{\text{pot}}(\vec{\mathbf{R}}) = V_{NM} + \frac{1}{2} V_D (\rho \nabla^2 \rho - |\vec{\nabla} \rho|^2) + \frac{\rho}{2} V_E \left(\frac{6}{5} k_F^2 \rho - 2\tau + \frac{1}{2} \nabla^2 \rho \right). \quad (2.7)$$

The expression of \mathcal{H}_{pot} has two distinct parts

with

$$g(k_{FS}) = \frac{35}{2(k_{FS})^3} j_3(k_{FS}). \quad (2.11)$$

Negele and Vautherin then proceed to eliminate the $\nabla^2 \rho$ terms by an integration by parts. In the case of a complex effective interaction, this implies the appearance of v^{ST} derivatives with respect to both ρ and τ . In order to avoid any derivative here we keep the $\nabla^2 \rho$ terms.

We introduce the following notation:

$$A = V_{NM} + \frac{3}{5} \left[\frac{3\pi^2}{2} \right]^{2/3} \rho^{8/3} V_E, \quad (2.12)$$

$$B = -\rho V_E, \quad (2.13)$$

$$C = -\frac{1}{2} V_D, \quad (2.14)$$

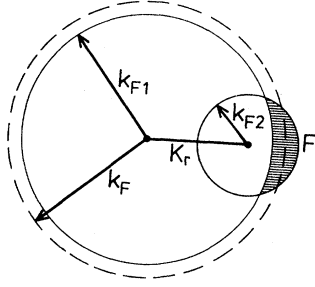


FIG. 1. A deformed Fermi sea used in the local description of a heavy ion collision as the collision of two nuclear matter systems.

$$D = \frac{1}{2}\rho(V_D + \frac{1}{2}V_E), \quad (2.15)$$

where A , B , C , and D are complex quantities, which depend on ρ , $\tau^{(2)}$, and the incident energy. Then the potential energy density (2.7) becomes

$$\mathcal{H}_{\text{pot}}(\vec{R}) = A + B\tau^{(2)} + C(\vec{\nabla}\rho)^2 + D\nabla^2\rho. \quad (2.16)$$

At this point we stress that the potential energy density (2.16) depends on the intrinsic kinetic energy density $\tau^{(2)}$ defined in Eq. (3.15) instead of the kinetic energy density τ as introduced by Negele and Vautherin.²² The difference comes from the fact that we deal with a moving system while Ref.

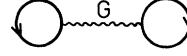


FIG. 2. Brueckner-Hartree-Fock contribution to the binding energy of the Fermi sea depicted in Fig. 1. The wiggly line depicts the Brueckner reaction matrix G .

22 treats a static case. The replacement of τ by $\tau^{(2)}$ appears as a consequence of preserving the Galilean invariance of the interaction.²³

III. THE BINDING ENERGY OF NUCLEAR MATTER FOR A NEARLY SPHERICAL FERMI SEA

As it will turn out in Sec. IV, it is useful to study the $\tau^{(2)}$ dependence of the imaginary part of the binding energy for a nearly spherical Fermi sea. The present analysis takes place in the momentum space and the density and the incident relative momentum K_r , given by the separation distance between the centers of the two spheres constituting the Fermi sea shown in Fig. 1 are fixed quantities. The intrinsic kinetic energy density $\tau^{(2)}$ is then uniquely determined by the radii of the two spheres.

In the Brueckner-Hartree-Fock (BHF) approximation, the potential energy of nuclear matter is given by the diagram of Fig. 2. It can be easily shown²⁴ that its imaginary part is proportional to the integral

$$\text{Im}V_{\text{BHF}} \propto \int d\vec{k}_1 d\vec{k}_2 d\vec{k}_3 d\vec{k}_4 |\langle \vec{k}_1 \vec{k}_2 | G(\omega_1 + \omega_2) | \vec{k}_3 \vec{k}_4 \rangle_A|^2 \delta(\omega_1 + \omega_2 - \omega_3 - \omega_4), \quad (3.1)$$

where the momenta \vec{k}_1 and \vec{k}_2 are inside the deformed Fermi sea F of Fig. 1, while \vec{k}_3 and \vec{k}_4 are outside it, and G is the Brueckner reaction matrix. The single particle energies ω_i are defined as

$$\omega_i = \frac{\hbar^2 k_i^2}{2m} + U(k_i), \quad (3.2)$$

where U is a continuous auxiliary potential.²⁴ For any \vec{k} integration, one has

$$\int d\vec{k} = \int k^2 dk d\hat{k} = \int k^2(\omega) \frac{dk}{d\omega} d\omega d\hat{k}, \quad (3.3)$$

where we have shifted from $k = |\vec{k}|$ to ω as the integration variable. This causes no problem since $\omega(k)$ is a monotonously increasing function of k . Hence, we can write

$$\text{Im}V_{\text{BHF}} \sim \int d\omega_1 d\omega_2 d\omega_3 d\omega_4 I(\omega_1, \omega_2, \omega_3, \omega_4) \times \delta(\omega_1 + \omega_2 - \omega_3 - \omega_4) \quad (3.4)$$

with

$$I(\omega_1, \omega_2, \omega_3, \omega_4) = \prod_{i=1}^4 \frac{dk_i}{d\omega_i} k_i^2 \int \prod_{i=1}^4 d\hat{k}_i |\langle \vec{k}_1 \vec{k}_2 | G(\omega_1 + \omega_2) | \vec{k}_3 \vec{k}_4 \rangle_A|^2. \quad (3.5)$$

Let us consider the Fermi sea of Fig. 1 and denote by ω_{F_1} the energy associated with the momentum k_{F_1} and by $\omega_{F_1} + \eta$ that of $K_r + k_{F_2}$. The quantity η is small compared to ω_{F_1} since the Fermi sea is nearly spherical.

Since ω_3 and ω_4 are greater than ω_{F_1} , the δ function in Eq. (3.4) vanishes except when \vec{k}_1 or/and \vec{k}_2 lie in-

side the dashed region called Z in Fig. 1. We thus have to consider two cases.

Case 1. Only one of the momenta \vec{k}_1 and \vec{k}_2 is inside Z . Let us consider that \vec{k}_1 is outside Z while \vec{k}_2 is inside it. Since all the above expressions are symmetrical in \vec{k}_1 and \vec{k}_2 , the case in which \vec{k}_1 is inside Z and \vec{k}_2 is outside it would yield the same result. The contribution to (3.4) is

$$(\text{Im}V_{\text{BHF}})_1 \sim \int_0^{\omega_{F1}} d\omega_1 \int_{\omega_{F1}}^{\omega_{F1}+\eta} d\omega_2 \int_{\omega_{F1}}^{\infty} d\omega_3 \int_{\omega_{F1}}^{\infty} d\omega_4 I(\omega_1, \omega_2, \omega_3, \omega_4) \delta(\omega_1 + \omega_2 - \omega_3 - \omega_4), \quad (3.6)$$

where we have specified the integration limits. It is, however, clear that the δ function imposes further restrictions over the range of integration of ω_1 , ω_3 , and ω_4 . One can easily see that in fact, the integration limits are restricted to

$$\begin{aligned} \omega_{F1} - \eta < \omega_1 < \omega_{F1}, \\ \omega_{F1} < \omega_2 < \omega_{F1} + \eta, \\ \omega_{F1} < \omega_3 < \omega_{F1} + \eta. \end{aligned} \quad (3.7)$$

The function $I(\omega_1, \omega_2, \omega_3, \omega_4)$ can thus be approxi-

$$(\text{Im}V_{\text{BHF}})_2 \sim \int_{\omega_{F1}}^{\omega_{F1}+\eta} d\omega_1 \int_{\omega_{F1}}^{\omega_{F1}+\eta} d\omega_2 \int_{\omega_{F1}}^{\infty} d\omega_3 \int_{\omega_{F1}}^{\infty} d\omega_4 I(\omega_1, \omega_2, \omega_3, \omega_4) \delta(\omega_1 + \omega_2 - \omega_3 - \omega_4) \quad (3.9)$$

and the further restrictions imposed by the δ function give

$$\begin{aligned} \omega_3 < \omega_{F1} + 2\eta, \\ \omega_4 < \omega_{F1} + 2\eta. \end{aligned} \quad (3.10)$$

Therefore the function $I(\omega_1, \omega_2, \omega_3, \omega_4)$ can again be approximated by $I(\omega_{F1}, \omega_{F1}, \omega_{F1}, \omega_{F1})$ and taken outside the integral sign. Explicit integration then yields

$$\begin{aligned} (\text{Im}V_{\text{BHF}})_2 &\sim I(\omega_{F1}, \omega_{F1}, \omega_{F1}, \omega_{F1}) \eta^3 \\ &\sim I(\omega_{F1}, \omega_{F1}, \omega_{F1}, \omega_{F1}) \\ &\quad \times [\omega(K_r + k_{F2}) - \omega(k_{F1})]^3, \end{aligned} \quad (3.11)$$

i.e., the same as in case 1.

Therefore, one has

$$\text{Im}V_{\text{BHF}} \sim [\omega(K_r + k_{F2}) - \omega(k_{F1})]^3. \quad (3.12)$$

Let us define k_F as the radius of the spherical Fermi sea corresponding to the fixed density ρ . One can write

$$\begin{aligned} k_{F1} &= k_F - \delta_1, \\ K_r + k_{F2} &= k_F + \delta_2, \end{aligned} \quad (3.13)$$

where δ_1 and δ_2 are small with respect to k_F and the change in the Fermi sea is such as the density remains equal to ρ (constant volume). Then Eq.

is approximated by $I(\omega_{F1}, \omega_{F1}, \omega_{F1}, \omega_{F1})$ and be taken outside the integral sign in Eq. (3.6). The remaining integrations are then straightforward and yield

$$\begin{aligned} (\text{Im}V_{\text{BHF}})_1 &\sim I(\omega_{F1}, \omega_{F1}, \omega_{F1}, \omega_{F1}) \eta^3 \\ &\sim I(\omega_{F1}, \omega_{F1}, \omega_{F1}, \omega_{F1}) \\ &\quad \times [\omega(K_r + k_{F2}) - \omega(k_{F1})]^3. \end{aligned} \quad (3.8)$$

Case 2. Both \vec{k}_1 and \vec{k}_2 lie inside Z . The contribution to (3.4) is now

(3.12) can be written in leading order

$$\text{Im}V_{\text{BHF}} \sim (\delta_1 + \delta_2)^3. \quad (3.14)$$

We have now to relate δ_1 and δ_2 to the variation of the intrinsic kinetic energy density $\tau^{(2)}$ when one goes from the spherical Fermi sea of radius k_F to the deformed sea F of Fig. 1.

The intrinsic kinetic energy density $\tau^{(2)}$ is defined as¹⁰

$$\tau^{(2)} = \tau - \rho k_G^2, \quad (3.15)$$

where ρ is the density, τ is the kinetic energy density given by

$$\tau = \frac{1}{V} \sum_{\vec{k} \sigma \tau} k^2, \quad (3.16)$$

and \vec{k}_G is the mean momentum per nucleon

$$\vec{k}_G = \frac{1}{N} \sum_{\vec{k} \sigma \tau} \vec{k}. \quad (3.17)$$

In Eqs. (3.16) and (3.17), the \vec{k} summations extend over the deformed Fermi sea F , σ and τ are the spin and isospin degrees of freedom, V is the volume of the box in which the system is contained, while N is the total number of nucleons. As usual V and N tend to infinity with

$$\frac{N}{V} = \rho = \text{constant}. \quad (3.18)$$

The intrinsic kinetic energy density $\tau^{(2)}$ defined

above represents the same quantity as that given by formula (6) of Ref. 21.

Denoting by Δx the variation of any quantity x when one goes from the spherical Fermi sea to the deformed one depicted in Fig. 1, one has

$$\Delta\tau^{(2)} = \Delta\tau - (\rho + \Delta\rho)(\Delta k_G)^2, \quad (3.19)$$

because $k_G = 0$ for a spherical Fermi sea (static case). By explicit calculation we obtain up to second order in δ_i

$$\begin{aligned} \Delta\rho \simeq & -\frac{2}{\pi^2} k_F^2 \delta_1 + \frac{1}{2\pi^2} k_F \left[3 + \frac{k_F}{K_r} \right] \delta_1^2 \\ & + \frac{k_F}{2\pi^2} \left[\frac{k_F}{K_r} - 1 \right] \delta_2^2 \\ & + \frac{k_F}{\pi^2} \left[\frac{k_F}{K_r} - 1 \right] \delta_1 \delta_2 + \dots \end{aligned} \quad (3.20)$$

Equation (3.20) shows that δ_1 and δ_2 cannot be of the same order of magnitude. The reason is that the density must remain constant and the constraint $\Delta\rho = 0$ would imply $\delta_i = 0$, i.e., no deformation at all. Therefore, the constraint $\Delta\rho = 0$ imposes

$$\delta_1 = 0(\delta_2^2). \quad (3.21)$$

Hence, up to third order in δ_2 , a consistent approximation to $\Delta\rho$ is provided by

$$\begin{aligned} \Delta\rho = & -\frac{2}{\pi^2} k_F^2 \delta_1 + \frac{k_F}{2\pi^2} \left[\frac{k_F}{K_r} - 1 \right] \delta_2^2 \\ & + \frac{k_F}{\pi^2} \left[\frac{k_F}{K_r} - 1 \right] \delta_1 \delta_2 \\ & + \frac{1}{2\pi^2} \left[\frac{k_F}{K_r} - \frac{1}{3} \right] \delta_2^3. \end{aligned} \quad (3.22)$$

The variation of the intrinsic kinetic energy density $\tau^{(2)}$ is then related to the variation $\Delta\rho$ of Eq. (3.22) by

$$\begin{aligned} \Delta\tau = & k_F^2 \left[\Delta\rho + \frac{1}{3\pi^2} \left[\frac{k_F}{K_r} - 1 \right] \delta_2^3 \right. \\ & \left. + 0(\delta_2^4) + \dots \right], \end{aligned} \quad (3.23)$$

where the term $0(\delta_2^4)$ also contains the variation of k_G^2 given by

$$(\Delta k_G)^2 = \left[\frac{k_F^2}{2\rho\pi^2} \left[\frac{k_F}{K_r} - 1 \right] \delta_2^2 \right]^2 + \dots \quad (3.24)$$

Hence, when $\Delta\rho = 0$, we have in the lowest order

$$\Delta\tau^{(2)} \simeq \frac{k_F^2}{3\pi^2} \left[\frac{k_F}{K_r} - 1 \right] \delta_2^3. \quad (3.25)$$

By comparing Eqs. (3.14) and (3.25) and taking into account Eq. (3.21), we get

$$\text{Im}V_{\text{BHF}} \sim \Delta\tau^{(2)}, \quad (3.26)$$

which is the main result of this section and will be used as a basic argument in the next section.

IV. THE PARAMETRIZED FORM OF DME COEFFICIENTS

We have computed the A , B , C , and D coefficients of Eq. (2.16) for $K_r = 0, 0.5$, and 1 fm^{-1} /nucleon and for a series of spherical and deformed Fermi seas. In view of possible future ap-

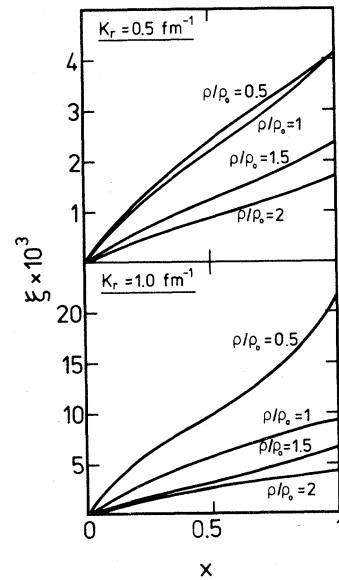


FIG. 3. The ratio $\xi = \text{Im}A/\text{Re}A$ for various densities and two K_r values as a function of x defined by Eq. (4.1). $\rho_0 = 0.17 \text{ nucleon/fm}^3$ is the normal nuclear matter density.

plications, it is useful to provide a simple parametrization of their dependence on ρ and $\tau^{(2)}$. In the following, \mathcal{C} will designate any of the A, B, C , and D coefficients.

A. $\tau^{(2)}$ parametrization

It turns out that the dependence on K_r and $\tau^{(2)}$ of the real part of any \mathcal{C} coefficient is negligible and therefore we only have to discuss the $\tau^{(2)}$ parametrization of $\text{Im}\mathcal{C}$. It is useful to define the ρ dependent ratio

$$x = \frac{\tau^{(2)} - \tau_{\min}^{(2)}}{\tau_{\max}^{(2)} - \tau_{\min}^{(2)}} = \frac{\Delta\tau^{(2)}}{\tau_{\max}^{(2)} - \tau_{\min}^{(2)}}, \quad (4.1)$$

where $\tau_{\min}^{(2)}$ and $\tau_{\max}^{(2)}$ are the minimum and maximum intrinsic kinetic energies associated with a deformed Fermi sea of a given density ρ . The value $\tau_{\min}^{(2)}$ corresponds to a spherical Fermi sea and gives $x=0$. The other extreme $\tau_{\max}^{(2)}$ implies $x=1$ and corresponds to a deformed Fermi sea composed of two spheres of equal radii having their centers separated by a distance K_r .

At present we wish to make use of the result obtained in the previous section. For a small deformation of the Fermi sea, i.e., small x , expression (3.25) indicates that the imaginary part of all \mathcal{C}

coefficients is proportional to x . Parametrizing the remaining dependence on x by a second degree polynomial we take the following expression for $\text{Im}\mathcal{C}$:

$$\text{Im}\mathcal{C} = x(I_1 + I_2x + I_3x^2) \quad (4.2)$$

and find values of the coefficients I_n ($n=1-3$) which reproduce the exact results within 3%. We note that each I_n depends on K_r and ρ . The ρ dependence is parametrized below. In Figs. 3–6, we plot the ratio

$$\xi = \frac{\text{Im}\mathcal{C}}{\text{Re}\mathcal{C}}$$

as a function of x for a series of values of ρ and K_r . Parametrization (4.2) is used for $\text{Im}\mathcal{C}$. These figures are very much reminiscent of Fig. 3 of Ref. 21 where the x dependence of the entire imaginary part of the Skyrme-type interaction had been found numerically. The present parametrization is more detailed than that of Ref. 21 and gives an explicit dependence on $\tau^{(2)}$ of the imaginary part of the energy density.

B. ρ parametrization

We now discuss the ρ parametrization of $\text{Re}\mathcal{C}$ and of the I_n ($n=1-3$) coefficients appearing in Eq. (4.2). As can be seen from Eqs. (2.8), (2.12),

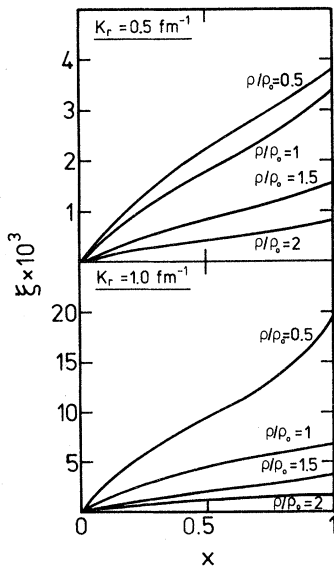


FIG. 4. Same as Fig. 3, but for $\xi = \text{Im}B/\text{Re}B$.

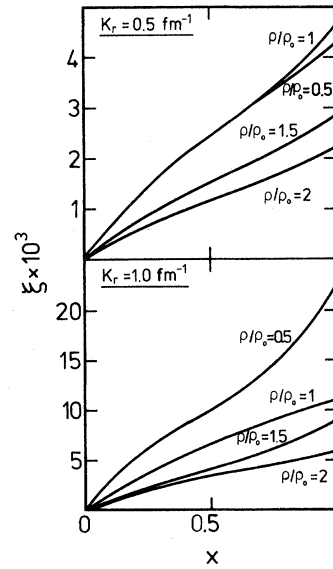


FIG. 5. Same as Fig. 3, but for $\xi = \text{Im}C/\text{Re}C$.

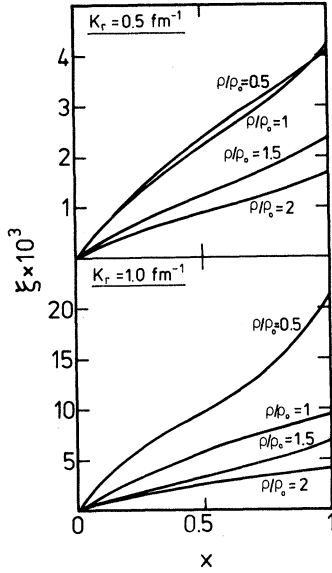


FIG. 6. Same as Fig. 3, but for $\xi = \text{Im}D/\text{Re}D$.

(2.13), and (2.15), a ρ^2 factor can be extracted from the ρ dependence of A , while a ρ factor can be extracted from that of B and D . By parametrizing the remaining ρ dependence by a cubic polynomial, we can write

$$\text{Re}\mathcal{C} = \rho^\alpha (R_1 + R_2\rho + R_3\rho^2 + R_4\rho^3) \quad (4.3)$$

and

$$I_n = \rho^\alpha (I_{n1} + I_{n2}\rho + I_{n3}\rho^2 + I_{n4}\rho^3) \quad (n=1-3), \quad (4.4)$$

where the exponent α is equal to 2, 1, 0, and 1 for the coefficients A , B , C , and D , respectively. Density parametrizations analogous to (4.3) and (4.4) were also used in Refs. 9 and 22.

The numerical values of R_j and I_{nj} ($n=1-3$; $j=1-4$) of all \mathcal{C} coefficients are gathered together in Table I. For $K_r=0$, all I_{nj} vanish because in the static case the G matrix has no imaginary part.

V. APPLICATION TO THE OPTICAL POTENTIAL

In order to check the reliability of the density matrix expansion applied to a complex effective interaction, we have calculated the $^{16}\text{O}+^{16}\text{O}$ optical

potential as defined by Eq. (1.1), where we have used the expression (2.16) with the parametrizations found for A , B , C , and D .

The densities ρ and $\tau^{(2)}$ have been calculated with a two center shell model described in Ref. 3 and equivalent to Fließbach's model.²⁵

In this model the ground state of $^{16}\text{O}+^{16}\text{O}$ is described by a Slater determinant built from the single particle states

$$\begin{aligned} \psi_{\alpha(1)} &= \phi_{\alpha(1)} e^{ik[z+(D/2)]}, \\ \psi_{\beta(2)} &= \phi_{\beta(2)} e^{-ik[z-(D/2)]}, \end{aligned} \quad (5.1)$$

where $\phi_{\alpha(1)}$ and $\phi_{\beta(2)}$ are eigenstates of harmonic oscillator wells centered at $-(D/2)$ and $D/2$, respectively. The relation between the single particle momentum component k along the z axis and K_r , defined previously is

$$k = \frac{1}{2}K_r. \quad (5.2)$$

Owing to the fact that the single particle states $\psi_{\alpha(1)}$ and $\psi_{\beta(2)}$ are not orthogonal, we have

$$\rho = \sum_{\beta(j), \alpha(i)} B_{\beta(j), \alpha(i)}^{-1}(D, k) \psi_{\alpha(i)}^* \psi_{\beta(j)}, \quad (5.3)$$

$$\tau = \sum_{\beta(j), \alpha(i)} B_{\beta(j), \alpha(i)}^{-1}(D, k) \vec{\nabla} \psi_{\alpha(i)}^* \vec{\nabla} \psi_{\beta(j)}, \quad (5.4)$$

and

$$\begin{aligned} \vec{k}_G = \frac{1}{2i\rho} \sum_{\beta(j), \alpha(i)} B_{\beta(j), \alpha(i)}^{-1}(D, k) \\ \times (\psi_{\alpha(i)}^* \vec{\nabla} \psi_{\beta(j)} - \vec{\nabla} \psi_{\alpha(i)}^* \psi_{\beta(j)}), \end{aligned} \quad (5.5)$$

where

$$B_{\beta(j), \alpha(i)} = \langle \psi_{\beta(j)}, \psi_{\alpha(i)} \rangle. \quad (5.6)$$

The results (full curves) are presented in Figs. 7 and 8 for the real and imaginary parts of V_{opt} , respectively. We compare them with the "exact" computation of Ref. 13 (dashed curves). The agreement for $\text{Im}V_{\text{opt}}$ is very good at all separation distances.

For the discussion of the real part it is useful to roughly divide the range of the separation distance R into two intervals. Let us call R_0 the distance at which $\text{Re}V_{\text{opt}}$ has an inflection point.

(a) $R > R_0$. This interval is dominated by the nuclear surface properties of the interaction because in the region where the nuclei interpenetrate the

TABLE I. The real R_j and imaginary I_{nj} parts of the DME coefficients A , B , C , and D defined by Eqs. (4.3) and (4.4). Note that R_j does not depend on K_r .

\mathcal{C}		$j=1$	$j=2$	$j=3$	$j=4$	
A	R_j	-519.42	1936.5	-5391.2	6265.3	
	$K_r=0.5$	I_{1j}	-1.7061	-22.876	175.19	-289.25
		I_{2j}	-0.0639	38.424	-227.17	349.65
		I_{3j}	1.0509	-36.367	191.34	-282.25
	$K_r=1.0$	I_{1j}	-30.761	282.88	-950.54	1086.1
		I_{2j}	55.802	-671.27	2707.1	-3541.0
		I_{3j}	-47.766	623.59	-2649.9	3600.5
	B	R_j	178.24	-1058.2	3359.3	-3969.4
		$K_r=0.5$	I_{1j}	0.89300	-1.6991	-13.110
I_{2j}			-0.30740	-4.2111	34.202	-57.614
I_{3j}			-0.12053	6.5022	-36.914	56.152
$K_r=1.0$		I_{1j}	9.1548	-91.622	319.86	-376.59
		I_{2j}	-14.065	163.45	-634.96	808.30
		I_{3j}	11.292	-141.52	578.26	-763.18
C		R_j	72.343	-385.83	1085.1	-1184.6
		$K_r=0.5$	I_{1j}	0.27056	1.6955	-16.537
	I_{2j}		-0.06102	-3.5555	22.764	-35.986
	I_{3j}		-0.07316	3.5791	-19.642	29.476
	$K_r=1.0$	I_{1j}	3.9753	-38.710	136.09	-161.54
		I_{2j}	-7.3330	91.173	-374.66	496.01
		I_{3j}	6.2272	-82.406	352.60	-480.85
	D	R_j	-116.90	650.39	-1925.0	2176.9
		$K_r=0.5$	I_{1j}	-0.49381	-1.2707	19.815
I_{2j}			0.13787	4.6082	-31.314	50.390
I_{3j}			0.10329	-5.2046	28.871	-43.514
$K_r=1$		I_{1j}	-6.2640	61.615	-216.05	255.68
		I_{2j}	10.849	-132.03	533.39	-698.08
		I_{3j}	-9.0502	117.79	-497.16	671.64

density is not higher than the saturation density of the nuclear matter. This can be easily seen within the proximity concept.^{26,27} In this interval the DME results are slightly higher than the exact results. The difference shows that the surface properties of the exact interaction have somewhat been altered by the DME. This is not surprising because the DME introduces a truncation of the higher order derivatives of the density matrix. To find the effect of this truncation it would be interesting to calculate the surface energy of semi-infinite slabs of nuclear matter both with the exact interaction and the energy density resulting from DME.

(b) $R < R_0$. At such separation distances the overlapping region has reached the nuclear matter density regime and the behavior of $\text{Re}V_{\text{opt}}$ is essentially given by the bulk properties of the nuclear matter. Owing to the independence of $\text{Re}\mathcal{C}$ on K_r and $\tau^{(2)}$ the discussion given below is valid for any K_r . For nuclear matter the DME approximation gives $E/A = -16.85$ MeV and

$$\frac{d^2}{d\rho^2} \left[\frac{E}{A} \right] = 451.9 \text{ MeV fm}^6$$

at the saturation density $\rho=0.2234 \text{ fm}^{-3}$. On the

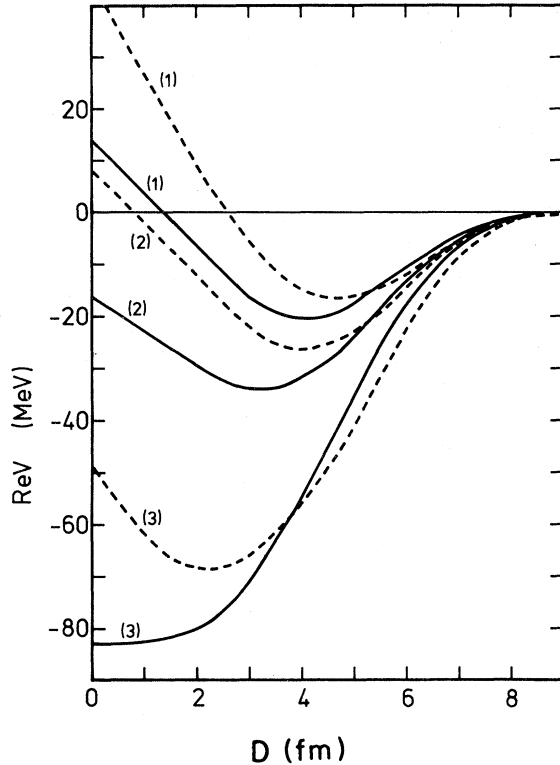


FIG. 7. A comparison between the density matrix expansion computation of $\text{Re}V_{\text{opt}}$ as a function of D (full lines) and the exact computation of Ref. 13 (dashed lines). The curves marked 1, 2, and 3 correspond to $K_F=0, 0.5,$ and 1 fm^{-1} , i.e., $E_{\text{lab}}=0, 83,$ and $332,$ respectively.

other hand the exact binding energy is -15.59 MeV and its second derivative takes the value 575.8 MeV fm^6 at a lower saturation density $\rho=0.1752 \text{ fm}^{-3}$. Therefore the DME overbinds the nuclear matter, as already noticed in Ref. 28, and alters the curvature at the saturation point. The changes it produces on the nuclear matter constants can explain the difference between the two results. Namely, $\text{Re}V_{\text{opt}}$ calculated with the DME reaches a deeper minimum at shorter separation distances than the exact $\text{Re}V_{\text{opt}}$. This is because the saturation Fermi momentum $k_F=1.49 \text{ fm}^{-1}$ given by the DME is larger than the exact one $k_F=1.37 \text{ fm}^{-1}$. Hence, in the first case, the saturation density is reached when the nuclei interpenetrate further, bringing in the extra attraction associated with the

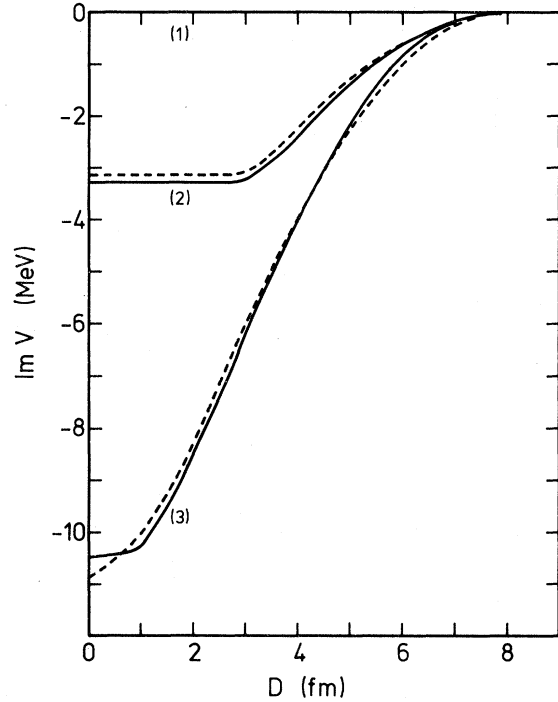


FIG. 8. Same as Fig. 3, but for $\text{Im}V_{\text{opt}}$.

overbinding mentioned above. Towards $R \rightarrow 0$, both potentials are linear, and the difference between their slope is consistent with the values found for

$$\frac{\partial^2}{\partial \rho^2} \left[\frac{E}{A} \right].$$

For the imaginary part, the $\tau^{(2)}$ dependence plays the dominant role and thus $\text{Im}V_{\text{opt}}$ is insensitive to the saturation density effects described above.

In conclusion, we believe to have found a reliable parametrization of a complex density functional to be used in the calculation of the heavy-ion optical potential. Our results are given at two different energies and can be applied to any pair of nuclei once the density and the kinetic energy density of the colliding system are known.

One of us (R.S.) acknowledges financial support from the Institut Interuniversitaire des Sciences Nucléaires.

¹K. A. Brueckner *et al.*, Phys. Rev. **171**, 1188 (1968).

²K. A. Brueckner *et al.*, Phys. Rev. **173**, 944 (1968).

³D. M. Brink and Fl. Stancu, Nucl. Phys. **A243**, 175 (1975).

⁴Fl. Stancu and D. M. Brink, Nucl. Phys. **A270**, 236

(1976).

⁵C. Ngô *et al.*, Nucl. Phys. **A240**, 353 (1975).

⁶C. Ngô *et al.*, Nucl. Phys. **A252**, 237 (1975).

⁷F. Beck, K. H. Müller, and K. S. Köhler, Phys. Rev. Lett. **40**, 837 (1978).

- ⁸K. H. Müller, *Z. Phys. A* 295, 79 (1980).
- ⁹B. Behera, K. C. Panda, and R. K. Satpathy, *Phys. Rev. C* 20, 683 (1979).
- ¹⁰T. Izumoto, S. Krewald, and A. Faessler, *Nucl. Phys. A* 341, 319 (1980).
- ¹¹T. Izumoto, S. Krewald, and A. Faessler, *Nucl. Phys. A* 357, 471 (1981).
- ¹²A. Faessler, T. Izumoto, S. Krewald, and R. Sartor, *Nucl. Phys. A* 359, 509 (1981).
- ¹³R. Sartor, A. Faessler, S. B. Khadkikar, and S. Krewald, *Nucl. Phys. A* 359, 467 (1981).
- ¹⁴R. Sartor and A. Faessler, *Nucl. Phys. A* 376, 263 (1982).
- ¹⁵G. R. Satchler and W. G. Love, *Phys. Rep.* 55, 183 (1979).
- ¹⁶J. P. Vary and C. B. Dover, *Phys. Rev. Lett.* 31, 1510 (1973).
- ¹⁷G. F. Bertsch, *Phys. Rev. C* 15, 713 (1977).
- ¹⁸E. S. Hernandez and S. A. Moszkowski, *Phys. Rev. C* 21, 929 (1980).
- ¹⁹N. J. Di Giacomo, J. C. Peng, and R. M. DeVries, *Phys. Lett.* 101B, 383 (1981).
- ²⁰D. A. Saloner and C. Toepffer, *Nucl. Phys. A* 283, 208 (1977).
- ²¹R. Sartor and Fl. Stancu, *Phys. Rev. C* 24, 2347 (1981).
- ²²J. W. Negele and D. Vautherin, *Phys. Rev. C* 5, 1472 (1972).
- ²³Y. M. Engel, D. M. Brink, K. Goeke, S. J. Krieger, and D. Vautherin, *Nucl. Phys. A* 249, 215 (1975).
- ²⁴J. P. Jeukenne, A. Lejeune, and C. Mahaux, *Phys. Rep.* 25C, 83 (1976).
- ²⁵T. Fliessbach, *Z. Phys.* 238, 329 (1970); 242, 287 (1971); 247, 117 (1971).
- ²⁶J. Błocki, J. Randrup, W. J. Swiatecki, and C. F. Tsang, *Ann. Phys. (N.Y.)* 105, 427 (1977).
- ²⁷D. M. Brink and Fl. Stancu, *Nucl. Phys. A* 299, 321 (1978).
- ²⁸D.W.L. Sprung, M. Vallières, X. Campi, and Che-Ming Ko, *Nucl. Phys. A* 253, 1 (1975).